Journal of Colloid and Interface Science **254,** 306–315 (2002)
doi:10.1006/jcis.2002.8594

Surface Modification of Sylgard-184 Poly(dimethyl siloxane) Networks by Ultraviolet and Ultraviolet/Ozone Treatment

Kirill Efimenko,* William E. Wallace,† and Jan Genzer*,[1]

*Department of Chemical Engineering, North Carolina State University, Raleigh, North Carolina 27695-7905; and †Polymers Division, National Institute of Standards and Technology, Gaithersburg, Maryland 20899-8541

Received March 5, 2002; accepted July 11, 2002

We report on the surface modification of Sylgard-184 poly(dimethyl siloxane) (PDMS) networks by ultraviolet (UV) radiation and ultraviolet/ozone (UVO) treatment. The effects of the UV light wavelength and ambient conditions on the surface properties of Sylgard-184 are probed using a battery of experimental probes, including static contact angle measurements, Fourier transform infrared spectroscopy, near-edge X-ray absorption fine structure, and X-ray reflectivity. Our results reveal that when exposed to UV, the PDMS macromolecules in the surface region of Sylgard-184 undergo chain scission, involving both the main chain backbone and the side groups. The radicals formed during this process recombine and form a network whose wetting properties are similar to those of a UV-modified model PDMS. In contrast to the UV radiation, the UVO treatment causes very significant changes in the surface and near-surface structure of Sylgard-184. Specifically, the molecular oxygen and ozone created during the UVO process interact with the UV-modified specimen. As a result of these interactions, the surface of the sample contains a large number of hydrophilic (mainly –OH) groups. In addition, the material density within the first ≈5 nm reaches about 50% of that of pure silica. A major conclusion that can be drawn from the results and analysis described in this work is that the presence of the silica fillers in Sylgard-184 does not alter the surface properties of the UVO- and UV-modified Sylgard-184. © 2002 Elsevier Science (USA)

Key Words: **Poly(dimethyl siloxane) networks; Sylgard-184; ultraviolet/ozone treatment; hydrophilic elastomers.**

INTRODUCTION

Since their introduction in the 1960s, silicone rubbers (SRs) have steadily gained market share from porcelain and glass as outdoor insulation and protective materials (1–3). The SR used in these applications is almost exclusively based on poly(dimethyl siloxane) (PDMS). PDMS is a low-density material with highly hydrophobic surface properties, low surface and bulk conductivity, and high fracture toughness over a wide temperature range. High hydrophobicity, contamination resistance, and long-term endurance made PDMS a very useful polymer for insulation, anticorrosion, and antifouling coatings.

Recent advances in nanotechnology ushered in a totally new paradigm for utilizing PDMS. Most of these studies used PDMS stamps fabricated from Sylgard-184, which is a commercially available two-component kit manufactured by Dow Corning (4). One of the novel technologies where Sylgard-184 PDMS has been an indispensable material is soft lithography (5). In soft lithography, a PDMS stamp with patterned relief structures on its surface is employed to generate motifs and structures with feature sizes ranging from few tens of nanometers to centimeters using one of these five techniques: microcontact printing, replica molding, microtransfer molding, micromolding in capillaries, and solvent-assisted micromolding. While in most applications Sylgard-184 was used without any further modification, in other cases the surface of Sylgard-184 had to be physically and/or chemically altered to achieve its desired properties. For example, several reports appeared that utilized the combination of oxygen plasma and subsequent chemical attachment of chlorosilane molecules to tune the surface energy of the PDMS stamp (6–11). This modification enabled microcontact printing of hydrophilic materials that would otherwise not adhere to the originally hydrophobic PDMS surface. In addition to soft lithography, physical or physicochemical surface modification of Sylgard-184 has been performed to fabricate PDMS nanostructures (12–15), to tune the surfaces of PDMS for adhesion (16) and fracture (17) studies and for mechanical assembly of oligomers (18, 19), and polymers (20), and to adjust the surface energies of microfluidic channels (21). To properly adjust the surface characteristics of Sylgard-184 in these applications, it is important to understand the changes the Sylgard-184 surface undergoes when exposed to various surface treatments.

It has long been recognized that in order to modify the surface properties of PDMS, various techniques can be utilized that involve physical (2, 22, 23) or chemical treatments or a combination of both (24, 25). Particularly oxygen plasma has been widely used to modify the surfaces of PDMS (26). These studies reported that oxygen plasma treatment propagated deep under the polymer surface (to about several hundred nanometers) (2, 27) and caused irreversible chemical changes in the near-surface region of PDMS (28). Analysis using X-ray photoelectron spectroscopy on plasma-treated samples revealed a rapid substitution of carbon atoms by oxygen atoms, which led to the formation of

[1] To whom correspondence should be addressed. E-mail: Jan_Genzer@ncsu.edu.

0021-9797/02 $35.00

hydrophilic surfaces. Simultaneously, the PDMS surface "skin" was converted into a thin and brittle silica-like layer. The creation of such a silica-like layer caused changes in the PDMS mechanical properties. Owen and Smith (27) reported on the formation of cracks in this surface silica-like layer and argued that these cracks allowed for the migration of low-molecular-weight uncrosslinked PDMS fragments to the surface (so-called "hydrophobic recovery"). However, it must be stressed that the fact that the bulk and the surface possess different elastic properties can, in some instances, be advantageous (12, 15, 18–20).

Another class of techniques used extensively to modify PDMS surfaces involves ultraviolet (UV) (29–31) or UV/ozone exposure (UVO) (32, 33). It was previously shown that when exposed to UV light or a combination of UV light and ozone, silicone rubbers underwent drastic surface chemical changes that were very similar to those induced by the oxygen plasma. However, the UV- and UVO-based modification processes are much slower (by about an order of magnitude) than the modification by plasma-based techniques. Several research groups studied intensively the structure of the UV- and/or UVO-modified PDMS surfaces. Contact angle experiments confirmed that the UVO-modified PDMS surfaces were polar consisting of –OH groups, although nonnegligible traces of carbon containing species even after very long treatment time were detected with X-ray photoelectron spectrometry (33). The researchers also reported on ellipsometric measurements on UVO-modified PDMS and argued that under irradiation a uniform silica-like layer was created that had a thickness around 10–30 nm.

Despite previous work on the physical modification of PDMS surfaces, no comprehensive study investigating the effects of physical modification of Sylgard-184 by UVO and UV radiation has appeared. The goal of this work is to carry out a detailed study of the effect of UV and UVO treatments on Sylgard-184 PDMS. One of the important questions we ask is to what extent, if any, does the presence of the silica fillers in Sylgard-184 alter the surface properties of the UVO- and UV-modified surfaces. It should be noted that all the surface characteristics of all the samples were examined immediately after UV or UVO treatment. The effect of the sample aging on the "hydrophobic recovery" will be addressed in a separate paper (34).

EXPERIMENTAL SECTION

Preparation of Sylgard-184 Poly(dimethyl siloxane) Network

All experiments were performed with Sylgard-184, an elastomeric PDMS kit manufactured by Dow Corning. The components for preparing the elastomers were supplied in two parts, Sylgard-184A and Sylgard-184B. These comprised primarily the components of a reaction mixture having vinyl end-capped oligomeric dimethyl siloxane, a methyl hydrosiloxane as crosslinking agent, and a platinum complex as a catalyst for the hydrosilation reaction (4). As obtained, Sylgard-184A and Sylgard-184B contained 30–60 and 10–30 wt%, respectively, of dimethylvinylated and trimethylated silica fillers, as reported by the manufacturer. A 10 : 1 Sylgard-184A/Sylgard-184B mixture by mass was prepared and stirred in a plastic cup using a glass rod. Trapped air bubbles resulting from the agitation of the mixture were removed by applying gentle vacuum ($\approx$100 Pa). For the X-ray reflectivity measurements, thin films (50–500 μm) of PDMS were created by spin-coating toluene solutions of the Sylgard-184A/Sylgard-184B mixtures on silicon wafers (5 cm in diameter) that were previously cleaned with ultraviolet/ozone treatment (see discussion below). The samples were subsequently cured at 65°C for 120 min to form the crosslinked PDMS network and further dried in vacuum for 24 h in order to remove any trapped toluene. For other measurements, the PDMS substrates were prepared by casting the Sylgard-184A/Sylgard-184B mixtures into a flat glass Petri dish and cured as described above. The cured flexible PDMS substrates ($\approx$0.5 mm thick) were then cut into 10 × 10-mm squares and soxhlet extracted for 72 h in toluene to remove uncrosslinked low-molecular-mass components from the network. Finally, the samples were dried under vacuum ($\approx$1 Pa) at 60°C for 24 h. Before use, the samples were stored under a nitrogen blanket to protect the sample surfaces from possible contamination.

Ultraviolet/Ozone (UVO) Treatment

The ultraviolet/ozone (UVO) treatment of the PDMS surface was carried out in a commercial UVO chamber (Jelight Company, Inc., Model 42) (35). UVO treatment is a photosensitized oxidation process in which the molecules of the treated material are excited and/or dissociated by the absorption of short-wavelength UV radiation. Atomic oxygen is simultaneously generated when molecular oxygen is dissociated by $\lambda_1 = 184.9$ nm and ozone by $\lambda_2 = 253.7$ nm. The 253.7-nm radiation is absorbed by most hydrocarbons and also by ozone. The organic products of this excitation react with atomic oxygen to form simpler, volatile molecules, which desorb from the surface. Therefore, when both wavelengths are present, atomic oxygen is continuously generated, and ozone is continually formed and destroyed. We carried out the UVO treatment using two different low-pressure mercury vapor grid lamps. Both lamps have an output of 28 mW/cm^2 at the distance 6 mm, as reported by the manufacturer, and have strong emissions at both λ_1 and λ_2; however, they differ in their spectral intensities emitted at λ_1 and λ_2. Specifically, the Standard Fused Quartz lamp transmits about 65% and the Suprasil UV lamp transmits about 90% of radiation at 184.9 nm. For this reason we refer to the Standard Fused Quartz and Suprasil lamps as UVO60 and UVO90, respectively, and the Sylgard-184 samples treated with these UVO lamps as Sylgard-184(UVO60) and Sylgard-184(UVO90), respectively. The Sylgard-184 specimens were placed into the UVO cleaner tray at a distance of about 5 mm from the UV source and exposed to the radiation from one side only for controlled periods of time. The pressure, temperature, and relative humidity in the chamber were maintained at 1 atm, 20°C, and 50–60%, respectively. To address the effect of the UV radiation alone on the modification

of the Sylgard-184 substrates, the chamber was purged with high purity nitrogen (99.999%) at constant gas flux during the UVO90 exposure; we refer to these samples as Sylgard-184(UV90).

Contact Angle Measurements Using the Sessile Drop Technique

The contact angle experiments were performed using a Ramé-Hart contact angle goniometer (Model 100-00), equipped with a CCD camera, and analyzed with the Ramé-Hart Imaging 2001 software (35). The advancing contact angles were read within 30 s after depositing 8 μL of the probe liquid on the substrate; the receding contact angles were determined by removing 4 μL from the droplet. Each data point reported in this paper represents an average of five measurements on different areas of the same sample and has an error less than $\pm 1.5^\circ$. We performed the contact angle measurements using two liquids: deionized water (DIW) ($R > 15$ MΩcm) and diiodomethane (Aldrich, used as supplied). As detailed later these contact angle data were used to estimate the surface energy of the solid (36).

Fourier Transform Infrared Spectroscopy in the Attenuated Total Reflection Mode

Fourier transform infrared spectroscopy in the attenuated total reflection mode (FTIR-ATR) was used for characterizing chemical changes that took place on the surface of the polymer. The spectra were recorded on a Digilab UMA-500 spectrometer equipped with a liquid-nitrogen-cooled MCT detector and the mirror speed was set at 0.3 cm/s (35). For each sample, 2048 scans were collected using a Ge-crystal detector with a resolution of 4 cm^{-1} under constant nitrogen flux to eliminate the effect of water vapor on the collected data. The data were analyzed using BioRad-IR software (35).

Near-Edge X-Ray Absorption Fine Structure

We used near-edge absorption fine structure (NEXAFS) to examine the surface and bulk chemistry (including bond densities) of the samples. The NEXAFS experiments were carried out on the NIST/Dow Soft X-ray Materials Characterization Facility at the National Synchrotron Light Source (NSLS) at Brookhaven National Laboratory (37, 38). NEXAFS involves the resonant soft X-ray excitation of a K or L shell electron to an unoccupied low-lying antibonding molecular orbital of σ symmetry, σ^*, or π symmetry, π^* (39). The initial state K shell excitation gives NEXAFS its element specificity, while the final-state unoccupied molecular orbitals provide NEXAFS with its bonding or chemical selectivity. A measurement of the intensity of NEXAFS spectral features thus allows for the identification of chemical bonds and determination of their relative population densities within the sample. The setup at the NSLS is capable of recording both the partial electron yield (PEY) NEXAFS and the fluorescence yield (FY) NEXAFS spectra. By simultaneously detecting both the PEY and FY NEXAFS signals, whose probing depths are $\approx$2 and $\approx$100 nm, respectively, the chemical information about the molecules on the surface and in the interior of the sample can be obtained. All spectra were collected at the "magic angle" of $\theta = 55^\circ$, where θ is the angle between the sample normal and the polarization vector of the X-ray beam (40, 41).

X-Ray Reflectivity

The specular X-ray reflectivity measurements were conducted in a θ–θ configuration with a 2-kW copper X-ray tube whose characteristic Kα line has an energy of 8.04 keV and a wavelength of 0.154 nm. Slits were used to define the incident and reflected X-ray beams. The incident beam had a divergence of 0.067°. No incident-beam monochromator was available on the instrument; instead an energy-sensitive detector with a resolution of approximately 200 eV was used. The reflectivity was scanned in an angular range from 0.1° to 2.5° giving momentum transfer of the X-rays normal to the surface in the range of 0.142 to 3.56 nm^{-1}. At X-ray wavelength of a few tenths of a nanometer, the refractive index of most materials is less than one. Hence, there exists a critical angle below which total external reflection of the radiation takes place. This critical angle, θ_c, can be approximated by $(\rho r_e \lambda^2/\pi)^{1/2}$, where ρ is the electron density or the number of electrons per unit volume of the material, λ is the X-ray wavelenght, and $r_e = 2.818 \times 10^{-15}$ m is the classical electron radius. All the angles used within the context of X-ray reflectivity are defined as grazing angles measured from the surface parallel. At any incident angle below θ_c total reflection occurs. In a typical specular X-ray reflectivity measurement, the reflected intensity is collected as a function of the incident angle as it is continuously varied through the critical angle. By modeling the result with a one-dimensional Schrödinger equation, the details of the electron density depth profile can be deduced. Free-surface roughness, interfacial roughness, and density variations in the thickness direction can also be determined using computer modeling to create electron-density depth profiles that best fit the experimental data. The information reported here represents an average over a lateral dimension of a few micrometers as dictated by the coherence length of the X-ray beam.

RESULTS AND DISCUSSION

Contact Angle Measurements

Contact angle measurements represent the easiest and quickest method for examining the properties of surfaces. We have used the sessile contact angle method to determine the wettability and ultimately the surface energies of Sylgard-184 networks before and after the UVO and UV/nitrogen (UV) treatments. In Fig. 1a we present the advancing contact angles of deionized water, $\theta_{adv,DIW}$, on Sylgard-184 samples treated with UVO60 (squares), UVO90 (circles), and UV90 (up-triangles) as a function of UVO treatment time, t_{UVO}. The data show that as t_{UVO} increases the initially hydrophobic substrate becomes more hydrophilic, suggesting that the surfaces contain an increasing

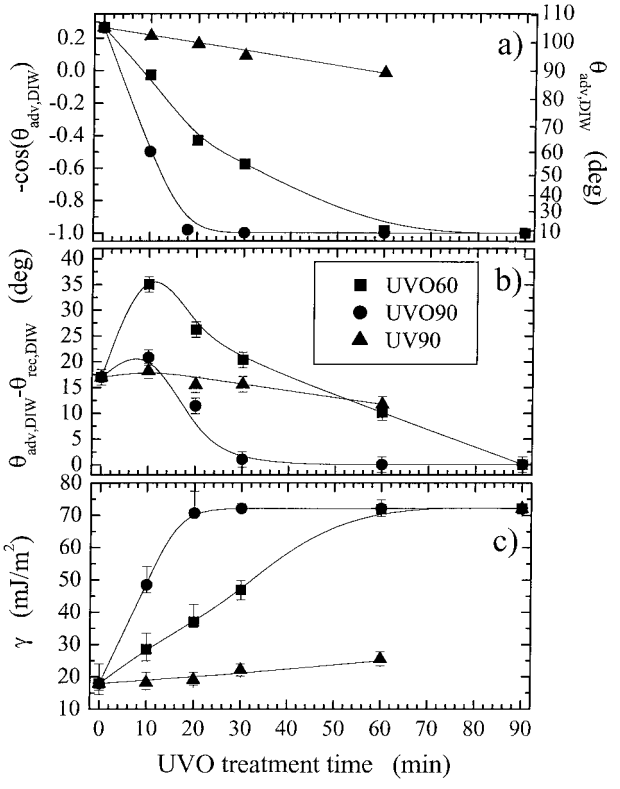

FIG. 1. Dependence of (a) the advancing contact angles of deionized water ($\theta_{\mathrm{adv,DIW}}$), (b) the contact angle hysteresis of deionized water ($\theta_{\mathrm{adv,DIW}} - \theta_{\mathrm{rec,DIW}}$), and (c) the surface energy on the UVO treatment time for Sylgard-184 exposed to UVO60 (squares), UVO90 (circles), and UV90 (up-triangles). In Part a each point represents an average of 5 measurements on various areas of the same sample (the error associated with these measurements is smaller than $\pm 1.5^\circ$). The lines are guides to the eye.

number of hydrophilic groups. The data in Fig. 1a show that there is a clear distinction between the UVO and UV treatments. Specifically, while the UV exposure results in a relatively moderate wettability increase, the UVO modification leads to a rapid increase of wettability on Sylgard-184. Moreover, it is evident that the UVO90 treatment is faster, relative to UVO60, in converting the hydrophobic PDMS substrate into a hydrophilic one, although at $t_{\mathrm{UVO}} = 90$ min both UVO60 and UVO90 substrates achieve virtually the same θ_{DIW} values. Interesting behavior is observed in the contact angle hysteresis, shown in Fig. 1b. The contact angle hysteresis (CAH), defined as the difference between the advancing and receding contact angles ($\theta_{\mathrm{adv,DIW}} - \theta_{\mathrm{rec,DIW}}$), is a measure of the physical and chemical nonuniformity of the surface. It is typically accepted that CAH smaller than $\approx 5^\circ$ is a signature of a fairly flat and chemically uniform substrate (36). The data show that even the untreated PDMS sample exhibits a nonnegligible CAH, however. Owen and coworkers reported (27, 42) that a large content of silica filler could affect the water CAH. Specifically, they argued that the water CAH for filled silicone elastomers was typically in the 20°–40° range, while that of unfilled PDMS was much lower ($<5^\circ$). From our data we can conclude that the silica fillers in the untreated Sylgard-184 sample are "buried" in the near-surface region and thus could influence the contact angle measurements.

Similar to the behavior of θ_{DIW} the CAH data can be divided into two groups, based on the treatment type. Specifically, the samples exposed to UV90 show a rather small decrease in the CAH. The UVO treatment leads to a nonmonotonous CAH time dependence. Specifically, for $t_{\mathrm{UVO}} < 10$ min CAH increases, while for $t_{\mathrm{UVO}} > 10$ min CAH decreases and eventually reaches very small values. Again there seems to be a difference between the samples treated with UVO60 and those exposed to UVO90. Specifically, while the CAH in Sylgard-184(UVO90) reaches its "final" value after ≈ 30 min, the CAH in Sylgard-184(UVO60) rises rapidly (for t_{UVO} it reaches $\approx 35^\circ$ a value that is nearly twice as large as the corresponding CAH in the Sylgard-184(UVO90) sample) and decreases only moderately with increasing UVO treatment time. Scanning force microscopy experiments revealed that the surfaces of the UVO- and UV-treated Sylgard-184 samples remained very flat even after $t_{\mathrm{UVO}} =$ 120 min (43). This observation is in accord with the results of Vasilets *et al.* who reported a decrease in the PDMS surface roughness during the exposure to UV under ambient conditions and under vacuum (29). The researchers attributed the decrease in roughness to the creation of additional crosslinks in the system. We return to the discussion concerning the CAH in the UVO- and UV-modified samples later in the text.

By measuring the contact angle data using two liquids the surface energies of the materials can be estimated (36). The surface energy of the substrate was calculated using the geometric mean approximation from the contact angle data of DI water and diiodomethane:

$$(1 + \cos\theta_{\mathrm{w}})\left(\gamma_{\mathrm{w}}^{\mathrm{d}} + \gamma_{\mathrm{w}}^{\mathrm{p}}\right) = 2\left(\sqrt{\gamma_{\mathrm{w}}^{\mathrm{d}}\gamma_{\mathrm{s}}^{\mathrm{d}}} + \sqrt{\gamma_{\mathrm{w}}^{\mathrm{p}}\gamma_{\mathrm{s}}^{\mathrm{p}}}\right), \qquad [1]$$

$$(1 + \cos\theta_{\mathrm{i}})\left(\gamma_{\mathrm{i}}^{\mathrm{d}} + \gamma_{\mathrm{i}}^{\mathrm{p}}\right) = 2\left(\sqrt{\gamma_{\mathrm{i}}^{\mathrm{d}}\gamma_{\mathrm{s}}^{\mathrm{d}}} + \sqrt{\gamma_{\mathrm{i}}^{\mathrm{p}}\gamma_{\mathrm{s}}^{\mathrm{p}}}\right). \qquad [2]$$

In Eqs. [1] and [2], the subscripts w, i, and s correspond to the DIW, diiodomethane, and the probed surface, respectively. The superscripts d and p represent the dispersive and polar components of the surface energy, respectively. Using the tabulated values of the dispersive and polar components of the surface energy ($\gamma_{\mathrm{w}}^{\mathrm{d}} = 21.6$ mJ/m^2, $\gamma_{\mathrm{w}}^{\mathrm{p}} = 50.4$ mJ/m^2, $\gamma_{\mathrm{i}}^{\mathrm{d}} = 47.7$ mJ/m^2, and $\gamma_{\mathrm{i}}^{\mathrm{p}} = 2.3$ mJ/m^2)$\gamma_{\mathrm{w}}^{\mathrm{p}}$ and $\gamma_{\mathrm{w}}^{\mathrm{p}}$ were calculated from Eqs. [1] and [2]. The dependence of the total surface energies of the substrates ($=\gamma_{\mathrm{w}}^{\mathrm{d}} + \gamma_{\mathrm{w}}^{\mathrm{p}}$) as a function of t_{UVO} for UVO60 (squares), UVO90 (circles), and UV90 (up-triangles) Sylgard-184 samples is shown in Fig. 1c. The data in Fig. 1c show that with increasing t_{UVO} the surface energy of the substrates exposed to UVO increases from ≈ 19 mJ/m^2 to ≈ 72 mJ/m^2. This increase is very rapid for the UVO90 treatment (≈ 20 min to reach the maximum value) and more gradual for the UVO60 modification (≈ 60 min to reach the maximum value). Thus the conclusion we reach is that during the UVO exposure a large number of hydrophilic functionalities on the surface of Sylgard-184 are formed. The higher concentrations of ozone and atomic oxygen

generated using the Suprasil lamp are presumably responsible for the fact that the UVO90 treatment is more aggressive as compared to the UVO60 treatment. Our results also show that the UV90 leads to only moderate increase in the surface energy of the Sylgard-184 substrate. Specifically, even after ≈60 min the surface energy of the Sylgard-184(UV90) substrate increases to only ≈25.5 mJ/m^2. Thus unlike the UVO modification, the exposure of the Sylgard-184 surfaces to UV90 results in only a small number of surface hydrophilic groups.

FTIR-ATR Measurements

FTIR-ATR measurements can be used to elucidate information about the various chemical functionalities present in the unmodified Sylgard-184 PDMS and the UVO- and UV90-treated samples to a depth of several micrometers. In Fig. 2 we plot the FTIR-ATR data from (bottom to top) Sylgard-184(UVO60), Sylgard-184(UVO90), and Sylgard-184(UV90) collected at various UVO treatment times, t_{UVO}: 0 min (A), 10 min (B), and 60 min (C). PDMS exhibits a series of characterisitc IR bands (see Table 1) (44). Among the most intense are those associated with –CH_3 rocking and ≡Si–C≡ stretching (band 1 in Fig. 2, 785–815 cm^{-1}), ≡Si–OH stretching (band 2 in Fig. 2, 825–865 cm^{-1}), asymmetric Si–O–Si stretches (band 5 in Fig. 2, 1055–1090 cm^{-1}), symmetric –CH_3 deformations (band 7 in Fig. 2, ≈1245–1270 cm^{-1}), asymmetric Si–CH_3 stretches (band 8 in Fig. 2, ≈2950–2970 cm^{-1}), and asymmetric Si–OH stretches (band 9 in Fig. 2, 3050–3700 cm^{-1}). By inspecting the FTIR-ATR spectra in Fig. 2 several conclusions can be made about the Sylgard-184(UVO60) samples (bottom spectra in the B and C groups). With increasing t_{UVO} there is a decrease in the band intensity characteristic of the Si–O–Si signal (cf. band 5), indicating that some chain scission occurred in the PDMS network. Simultaneously, there is a decrease in the –CH_3 signals (bands 1, 7, and 8) that is accompanied by an increase in –OH signal (bands 2, 3, and 9), suggesting oxidative conversion of the –[$(CH_3)_2$Si–O]– molecules into more hydrophilic species. Feature-wise, the spectra for Sylgard-184(UVO90) look virtually identical to those from the Sylgard-184(UVO60) samples, suggesting that the UVO60 and UVO90 treatments led to similar structures. From the time dependence of signals in band 9 we see that as compared to UVO60, the UVO90 treatment is more efficient in creating the –OH groups. The top spectrum in each group represents the FTIR-ATR data collected from the Sylgard-184(UV90) samples. Similar to the UVO-modified specimens, in Sylgard-184(UV90) samples there is a decrease in the peak characteristic of the ≡Si–O–Si≡ signal with increasing t_{UVO}, indicating that some chain scission occurred in the PDMS network. There is also a decrease in the –CH_3 signal. However, in contrast to the UVO-treated PDMS, there is no indication of creating new –OH bonds (no or only very weak peaks can be found in the regions around 900 cm^{-1} and 3000–3700 cm^{-1}). Thus unlike the UVO treatment, the exposure of Sylgard-184 to the UV90 radiation does not seem to produce many hydrophilic –OH functionalities. In both UVO- and UV-treated samples there is a decrease in the Si–CH_3 signal (bands 1, 7, and 8); the number of the ≡Si–CH_3 bonds seems to decrease more rapidly in the UV-treated samples. While the number of the ≡Si–O–Si≡ links decreases in both UVO- and UV-modified specimens, it is much more pronounced in the latter material. Thus compared

TABLE 1
Assignment of IR Spectra of Sylgard-184(UVO60), Sylgard-184(UVO90), and Sylgard-184(UV90) Shown in Fig. 2

Peak in Fig. 2	IR region (cm^{-1})	Description
1	785–815	–CH_3 rocking and ≡Si–C≡ stretching in ≡Si–CH_3
2	825–865	≡Si–O stretching in ≡Si–OH
3	875–920	≡Si–O stretching in ≡Si–OH
4	1015–1150	In-phase and out-of-phase wagging vibrations of –(CH_2)– in ≡Si–$(CH_2)_2$–Si≡ and ≡Si–CH_2–Si≡
5	1055–1090	Asymmetric ≡Si–O–Si≡ stretching in [–$(CH_2)_2$Si–O–]$_x$
6	1100–1170	In-phase and out-of-phase wagging vibrations of –(CH_2)– in ≡Si–$(CH_2)_2$–Si≡
7	1245–1270	Symmetric –CH_3 deformation in ≡Si–CH_3
8	2950–2970	Asymmetric –CH_3 stretching in ≡Si–CH_3
9	3050–3700	–OH stretching in ≡Si–OH, possibly also in ≡C–OH (3610–3640 cm^{-1})

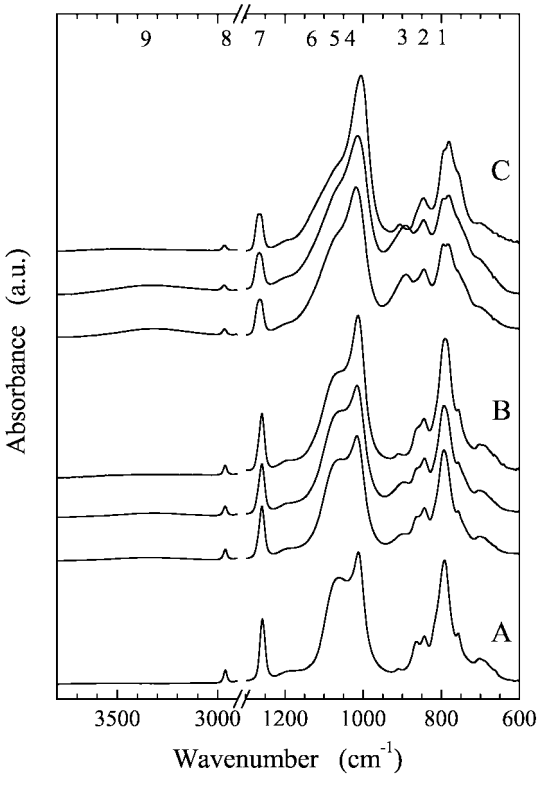

FIG. 2. FTIR-ATR spectra from Sylgard-184 treated for t_{UVO} equal to 0 min (A), 10 min (B), and 60 min (C) with (bottom to top) UVO60, UVO90, and UV90.

to the UVO treatment, the UV radiation is presumably more effective in scission of the main polymer backbone. The data in Fig. 2 also suggest that chain scission is accompanied by the creation of short hydrocarbon linkages in the UVO-modified Sylgard-184 samples (bands 4 and 6) (45). Overall, our results reiterate our previous conclusion, namely, that the UVO treatment is more effective in creating hydrophilic groups in Sylgard-184 as compared to the UV modification. Because of its poor surface sensitivity relative to other techniques, FTIR-ATR cannot be used to monitor the spatial distribution of the silica fillers in the subsurface region of Sylgard-184. However, the FTIR-ATR results may help to explain the behavior of the water CAH discussed previously. Specifically, we speculate that the temporal increase in the CAH at short UVO times can be associated with the surface damage of Sylgard-184, caused by the chain scission. With increasing t_{UVO}, the surface of Sylgard-184 becomes enriched in silica-like material (see below) and as a consequence the silica fillers may be expelled from or incorporated into the subsurface region leading to lower CAH values.

NEXAFS Measurements

While useful for identifying various chemical functionalities in materials, the probing depth of FTIR (typically ranging from a few hundreds of nanometers to several micrometers) is too large to discriminate between the chemical changes in UVO-modified Sylgard-184 in the near-surface region and those in the bulk. The NEXAFS setup at the Soft X-ray Materials Characterization Facility at NSLS is capable of simultaneously resolving chemical information on the sample surface and in the bulk by monitoring the partial electron yield (PEY; probing depth, ≈2 nm) and fluorescence yield (FY; probing depth, ≈100 nm) NEXAFS signals, respectively. Figures 3a and 3b depicts the 1s carbon K-edge PEY NEXAFS spectra collected from the Sylgard-184 treated with UVO60 and UVO90, respectively, at various UVO treatment times equal to 0 min (A), 20 min (B), and 120 min (C). The spectra were normalized such that the PEY intensities of the pre-edge and post-edge signals, assigned to be at 260.0 and 340.0 eV, respectively, were normalized to 0 and 1 on an arbitrary intensity scale, respectively. The NEXAFS spectra in Figs. 3a and 3b exhibit several characteristic peaks. Peak 1 (around $E = 291.0$ eV) can be assigned to the 1s $\rightarrow \sigma^*$ transition of the C–Si bond (46) and peak 2 ($E = 287.2$ eV) is associated with the 1s $\rightarrow \sigma^*$ transition of the C–H bond (39, 46). Finally, the set of peaks at energies below the carbon ionization edge (<288 eV; peak 3 in Fig. 3) corresponds to the second harmonic signal of oxygen. The data show that with increasing t_{UVO} the intensities of peaks 1 and 2 decrease while the intensity of peak 3 increases. This behavior results from breaking the Si–C and C–H bonds and the enrichment of the PDMS-modified surface with oxygen. While the decrease in the peak 1 and 2 signals is almost the same for both the UVO60- and UVO90-modified Sylgard-184 specimens, the intensity increase of the signal 3 is larger for the Sylgard-184(UVO90) samples. This behavior suggests

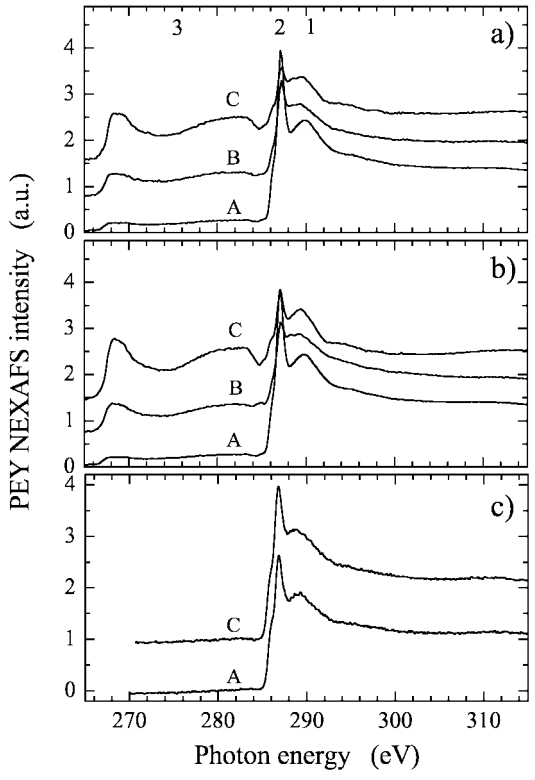

FIG. 3. Carbon K-edge PEY NEXAFS spectra from Sylgard-184 modified with (a) UVO60 and (b) UVO90 for t_{UVO} equal to 0 min (A), 20 min (B), and 120 min (C). Part c shows the carbon K-edge FY NEXAFS spectra from Sylgard-184 modified with UVO90 for t_{UVO} equal to 0 min (A) and 120 min (B). All spectra have been shifted vertically for clarity.

that the Sylgard-184 surfaces exposed to UVO90 were oxidized to an extent larger than that of those treated with UVO60. It is of great interest to find out how deep inside the sample the UVO and UV treatments penetrate. FY NEXAFS spectra collected from the UVO-treated samples treated for t_{UVO} ranging from 10 to 120 min (cf. Fig. 3c) are almost indistinguishable from that of an untreated Sylgard-184. Hence, by comparing the PEY and FY NEXAFS data we can conclude that the UVO treatment modifies mainly the surface and near-surface regions in Sylgard-184 but not the bulk.

Taking advantage of the superior sensitivity of PEY NEXAFS, we also performed a series of experiments exploring the detailed changes in the oxygen environment on the surfaces of UVO-treated Sylgard-184 samples. In Fig. 4a we show the oxygen K-edge PEY NEXAFS spectra from Sylgard-184(UVO90) treated for t_{UVO} equal to 0 min (A), 10 min (B), 20 min (C), 40 min (D), and 120 min (E). To understand the small changes in the shape of the main peak, we subtracted the oxygen K-edge PEY NEXAFS spectrum of unmodified Sylgard-184 from those of Sylgard-184(UVO90) samples treated for various t_{UVO}. These difference PEY NEXAFS spectra for Sylgard-184(UVO90) networks are shown in Fig. 4b. The data in Fig. 4b reveal the presence of two characteristic spectral regions (marked as 1 and 2)

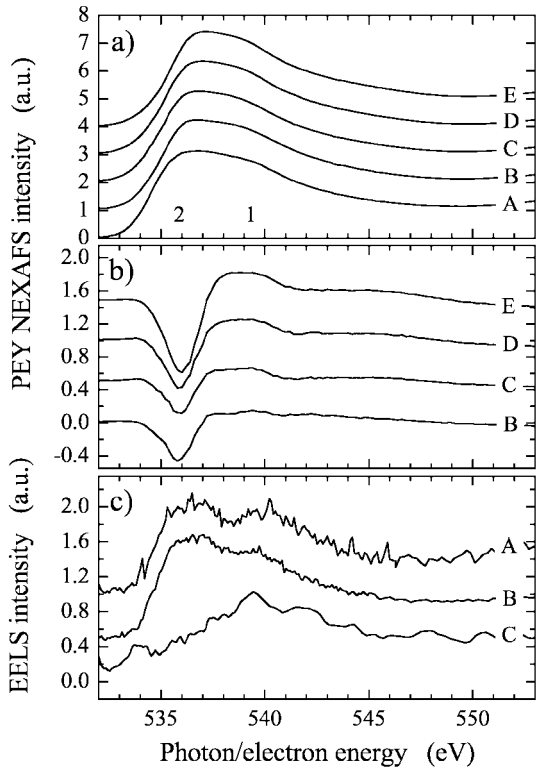

FIG. 4. Oxygen K-edge (a) PEY NEXAFS spectra; (b) difference PEY NEXAFS spectra (see text for explanation) from Sylgard-184(UVO90) treated for t_{UVO} equal to 0 min (A only in part a), 10 min (B), 20 min (C), 40 min (D), and 120 min (E); and (c) electron energy loss spectroscopy (EELS) data from cyclic-[O–Si$(CH_3)_2$]$_3$– (A), cyclic-[O–Si$(CH_3)_2$]$_4$– (B), and (phenyl)$_3$Si–OH (C) (46). All spectra have been shifted vertically for clarity.

whose intensities vary systematically with t_{UVO}. To interpret the information in NEXAFS difference spectra, we used electron energy loss spectroscopy (EELS) results from cyclic-[O–Si$(CH_3)_2$]$_3$– (A), cyclic-[O–Si$(CH_3)_2$]$_4$– (B), and (phenyl)$_3$Si–OH (C), shown in Fig. 4c (46, 47). The peaks around 536 and 540 eV in spectra A and B in Fig. 4c can be tentatively associated with the presence of ≡Si–O–Si≡ bonds. It must be noted that, in general, it is not easy to resolve a discrete ≡Si–O–Si≡ feature. The ≡Si–O–Si≡ bonds are "mostly but not totally" ionic, so σ^* character in these bonds is not very strong (48). Similarly, a broad peak at 539 eV in the spectrum of (phenyl)$_3$Si–OH (C) can be attributed to ≡Si–OH. Clearly, similarities exist between the data in Figs. 4b and 4c; hence, peaks 1 and 2 in Fig. 4b can be tentatively assigned to –OH and ≡Si–O– signals, respectively. The results presented in Fig. 4 reveal that during the UVO treatment, the number of surface ≡Si–O–Si≡ groups decreases and the number of surface –OH groups increases with increasing t_{UVO}. More work is currently underway to study these effects in greater detail (49).

X-Reflectivity Measurements

Specular X-ray reflectivity (XR) was used to depth profile the sample electron density in the direction perpendicular to the sample surface. The information reported here is an average over a lateral dimension of a few micrometers as dictated by the coherence length of the X-ray beam. In Fig. 5 we present the specular XR data collected from unmodified (open circles), UVO60 (closed squares), UVO90 (closed circles), and UV90 (closed up-triangles) modified Sylgard-184 samples. The UVO and UV90 samples were treated for 30 min. As mentioned earlier, below a certain critical wavevector there is a complete total external reflection of the radiation from the sample. Above that wavevector, the X-ray beam is only partially reflected. Hence the total detected X-ray intensity is a superposition of the various signals reflected at various depths inside the sample, where there is contrast in the electron scattering-length density. The details of the electron density depth profile can be deduced by modeling the experimental XR data with a one-dimensional Schrödinger equation. The inset in Fig. 5 depicts the best fits to the experimental XR data. These curves were obtained using computer modeling, allowing for the free-surface roughness, the interfacial roughness, the sample thickness, and the electron density inside the sample to vary. The depth profiles described here feature gentle gradients in the electron density. This is particularly hard to measure by X-ray reflectivity where abrupt changes in the density profile are most readily measured. For this reason it should be noted that the density profiles shown are qualitative and are best employed to show general trends in the PDMS behavior. The data show that the electron density in the unmodified Sylgard-184 is homogeneous with the value of 5×10^{-4} Å^{-2} corresponding to model PDMS (50). Furthermore, the surfaces were highly reflective, consistent with flat homogenous samples.

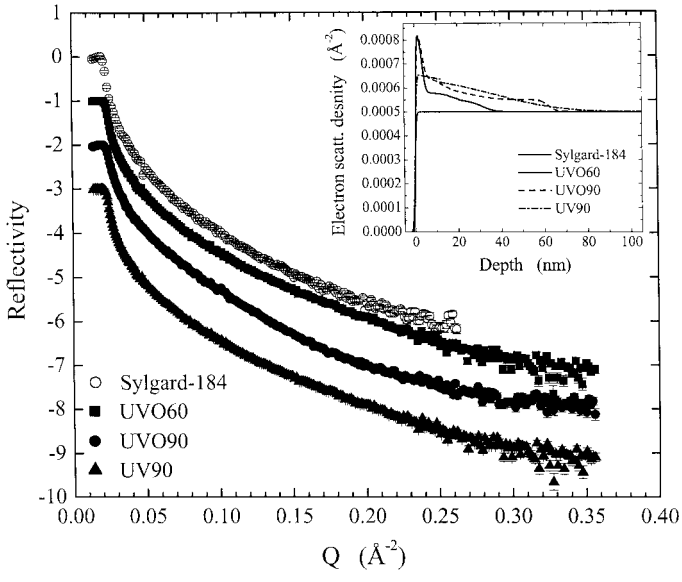

FIG. 5. X-ray reflectivity from untreated Sylgard-184 (open circles) and Sylgard-184 exposed to UVO60 (closed squares), UVO90 (closed circles), and UV90 (closed up-triangles) for $t_{UVO} = 30$ min. The data were shifted vertically for clarity. The inset depicts the corresponding X-ray electron scattering-length density squared profiles obtained by fitting the experimental X-ray reflectivity data.

The XR did not detect silica fillers at least in the subsurface region, where XR is most sensitive. This can be the case if either the fumed silica electron density is the same as PDMS or there are no filler particles within ≈5 nm of the surface. The data in the inset show that there is an increase in the electron density at the surface in the samples exposed to UVO. The density varies in a nonmonotonous way, being rather high within the first ≈5 nm (region 1), slowly decreasing over the next ≈40–60 nm (region 2) to reach the value corresponding to the untreated PDMS sample.

To learn how the electron density of the UVO- and UV-modified Sylgard-184 samples compared to that of pure silica, we normalize the electron density profiles obtained by fitting the experimental XR data on UVO- and UV/nitrogen-treated Sylgard-184 samples relative to that of an untreated Sylgard-184 and present the data in the form of a percentage of conversion to a silica-like structure. In Fig. 6 we show the conversion of the PDMS into silica as a function of the distance from the sample surface for untreated Sylgard-184 (thin dotted lines) and for Sylgard-184 treated with (a) UVO60, (b) UVO90, and (c) UV90 sources for t_{UVO} equal to 10 min (solid lines), 20 min (dashed lines), and 60 min (dash–dotted lines). The lines in Fig. 6 were obtained by normalizing the electron scattering-length density squared (ESD) profiles obtained from the XR measurements using the ESD values of silica (11.4×10^{-4} Å$^{-2} = 8.05 \times 10^{23}$ electrons/cm^3) and PDMS (5.0×10^{-4} Å$^{-2} = 3.53 \times 10^{23}$ electrons/cm^3) (50). Several conclusions can be drawn by inspecting the data in Fig. 6. First, at short t_{UVO} the modification of both UVO-modified samples extends only ≈10–20 nm below the surface. With increasing t_{UVO}, the PDMS-to-silica conversion increases within the first ≈5 nm beneath the surface and saturates at a value of ≈50%. This denser layer then gradually decays into the bulk over the next ≈30 nm and ≈60 nm for Sylgard-184(UVO60) and Sylgard-184(UVO90), respectively. The data for Sylgard-184(UV90) show that with increasing t_{UVO} the PDMS-to-silica conversion increases but in contrast to the UVO-treated Sylgard-184, this increase is much smaller (≈50% of that observed in the UVO samples) and leads to profiles monotonically decaying over ≈70 nm into the sample. We explain the different behavior observed in the UVO- and UV90-treated Sylgard-184 specimens as follows. The exposure of Sylgard-184 to UV leads to the formation of surface radicals. These radicals recombine forming various types of networks and terminal surface groups. In the absence of molecular oxygen and/or ozone, these moieties are composed of mainly hydrophobic species. However, when molecular oxygen and/or ozone are present, such as in case of the UVO treatment, these form large numbers of hydrophilic species, including free –OH groups and additional ≡Si–O–Si≡ linkages, eventually converting the first ≈5 nm within PDMS to a more dense material (≈50% density of pure silica). This dense subsurface layer becomes a diffusion barrier for the molecular oxygen and ozone and as a result the PDMS density at depths more than ≈10 nm below the surface is only ≈10% of that of pure silica. This conclusion is also supported by literature data on the diffusivity of oxygen in PDMS (typically ≈10^{-5} cm^2/s) (51) and silica (10^{-12}–10^{-19} cm^2/s, depending on preparation method) (52).

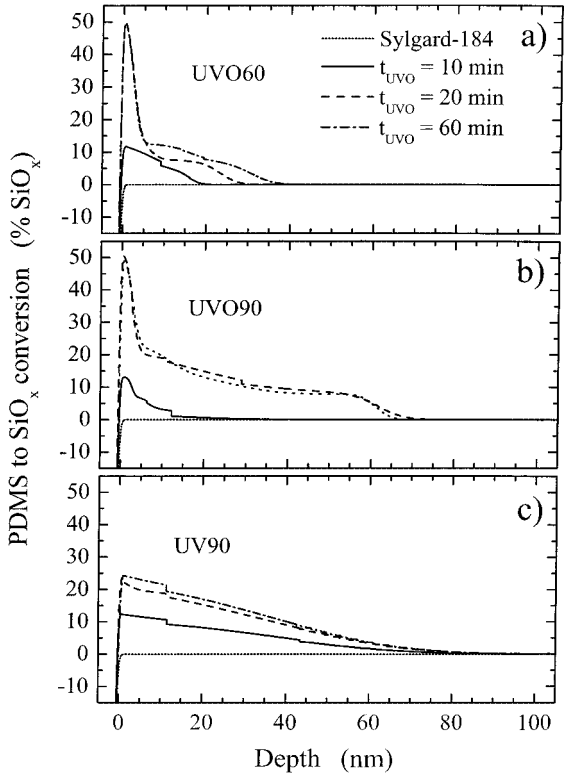

FIG. 6. PDMS-to-silica conversion as a function of the depth below the surface for Sylgard-184 treated with (a) UVO60, (b) UVO90, and (c) UV90 sources. Shown in each figure are the conversion curves for untreated Sylgard-184 (thin dotted lines) and that treated for t_{UVO} equal to 10 min (solid lines), 20 min (dashed lines), and 60 min (dash–dotted lines). The lines were obtained by normalizing the electron scattering-length density squared (ESD) profiles determined from the X-ray reflectivity measurements using the ESD values of silica (11.4×10^{-4} Å$^{-2} = 8.05 \times 10^{23}$ electrons/cm^3) and PDMS (5.0×10^{-4} Å$^{-2} = 3.53 \times 10^{23}$ electrons/cm^3) (50).

SUMMARY

In this work we have studied the effect of UV and UVO treatments on the modification of a Sylgard-184 poly(dimethyl siloxane) (PDMS) network. Our results showed that when exposed to UV, Sylgard-184 underwent chain scission, involving both main backbone and the side groups. The radicals formed during this process recombined, forming a network whose wetting properties were close to those of an untreated Sylgard-184. In contrast to the UV radiation, the UVO treatment caused very significant changes in the surface and subsurface structure of Sylgard-184, which contained a large number of hydrophilic groups (e.g., –OH). The material density within the first ≈5 nm of Sylgard-184, i.e., the region that was most affected by the UVO treatment, reached about 50% of that of silica. A major

conclusion that can be drawn from the results and analysis described in this work is that the presence of the silica fillers does not alter the surface properties of the UVO- and UV-modified Sylgard-184 specimens. Our results are in accord with previous studies on silica filler containing PDMS materials that concluded that the silica fillers were rarely seen in the subsurface region of oxygen plasma PDMS films (27, 42, 53, 54). In light of our results, we conclude that Sylgard-184 can be used as a convenient material for nanotechnology processes, such as those mentioned in the Introduction, that require nanometer scale control of their physical and chemical surface features.

ACKNOWLEDGMENTS

This research was supported by a Camille Dreyfus Teacher–Scholar Award, a 3M Non-Tenured Faculty Award, and funding provided by the NACE International. Partial support from the NSF Career Award, Grant DMR98-75256, is also gratefully acknowledged. NEXAFS experiments were carried out at the National Synchrotron Light Source, Brookhaven National Laboratory, which is supported by the U.S. Department of Energy, Division of Materials Sciences and Division of Chemical Sciences. The authors thank Dr. Daniel Fischer (NIST) for his assistance during the course of the NEXAFS experiments and Professor Stephen Urquhart (University of Saskatchewan, Canada) for many helpful discussions related to NEXAFS and EELS. We also thank Professor Stefan Franzen (NCSU's Department of Chemistry) for allowing us to use his FTIR–ATR spectrometer.

REFERENCES

1. Hall, J. F., *IEEE Trans. Power Delivery* **8,** 376 (1993).
2. Hillborg, H., and Gedde, U. W., *IEEE Trans. Dielectr. Electr. Insulation* **6,** 703 (1999).
3. Owen, M. J., *in* "Siloxane Polymers" (S. Clarson and J. A. Semlyen, Eds.), p. 309. Prentice Hall, Englewood Cliffs, NJ, 1993.
4. Product information on Sylgard-184 obtained from Dow Corning (this information can be retrieved from Dow Corning's web site at http://www.dowcorning.com).
5. Xia, Y., and Whitesides, G. M., *Annu. Rev. Mater. Sci.* **28,** 153 (1998); Xia, Y., and Whitesides, G. M., *Angew. Chem. Int. Ed.* **37,** 550 (1998); Xia, Y., Rogers, J. A., Paul, K. E., and Whitesides, G. M., *Chem. Rev.* **99,** 1823 (1999).
6. Xia, Y., and Whitesides, G. M., *Langmuir* **13,** 2059 (1997).
7. Kind, H., Bonard, J.-M., Emmenegger, C., Nilsson, L.-O., Hernadi, K., Maillard-Schaller, E., Schlapbach, Forró, L., and Kern, K., *Adv. Mater.* **11,** 1285 (1999).
8. Lahriri, J., Otsuni, E., and Whitesides, G. M., *Langmuir* **15,** 2055 (1999).
9. Yan, L., Huck, W. T. S., Zhao, X.-M., and Whitesides, G. M., *Langmuir* **15,** 1208 (1999).
10. Kind, H., Bonard, J.-M., Forró, L., Kern, K., Hernadi, K., Nilsson, L.-O., and Schlapbach, L., *Langmuir* **16,** 6877 (2000).
11. Martin, B. D., Brandow, S. L., Dressick, W. J., and Schull, T. L., *Langmuir* **16,** 9944 (2000).
12. Bowden, N., Brittain, S., Evans, A. G., Hutchinson, A. W., and Whitesides, G. M., *Nature* **393,** 146 (1998); Bowden, N., Huck, W. T. S., Paul, K., and Whitesides, G. M., *Appl. Phys. Lett.* **75,** 2557 (1999); Huck, W. T. S., Bowden, N., Onck, P., Pardoen, T., Hutchinson, A. W., and Whitesides, G. M., *Langmuir* **16,** 3497 (2000).
13. Rogers, J. A., Paul, K. E., Jackman, R. J., and Whitesides, G. M., *J. Vac. Sci. Technol. B* **16,** 59 (1998).
14. Schmid, H., Biebuyck, M., Michel, B., and Martin, O. J. F., *Appl. Phys. Lett.* **72,** 2379 (1998).
15. Chua, D. B. H., Ng, H. T., and Li, S. F. Y., *Appl. Phys. Lett.* **76,** 721 (2000).
16. Chaudhury, M. K., and Whitesides, G. M., *Langmuir* **7,** 1013 (1991); Chaudhury, M. K., and Whitesides, G. M., *Science* **255,** 1230 (1992); Chaudhury, M. K., and Owen, M. J., *J. Phys. Chem.* **97,** 5722 (1993).
17. Chaudhury, M. K., *J. Phys. Chem.* **103,** 6562 (1999).
18. Genzer, J., and Efimenko, K., *Science* **290,** 2130 (2000).
19. Efimenko, K., and Genzer, J., *Adv. Mater.* **13,** 1560 (2001).
20. Wu, T., Efimenko, K., and Genzer, J., *Macromolecules* **34,** 684 (2001).
21. See for example, Duffy, D. C., Schueller, O. J. A., Brittain, S. T., and Whitesides, G. M., *J. Micromech. Microeng.* **9,** 211 (1999); Folch, A., Hurtado, O., Schmidt, M., and Toner, M., *J. Biomechan. Eng.* **121,** 28 (1999).
22. Liston, E. M., Martinu, L., and Wertheimer, M. R., *in* "Plasma Surface Modification of Polymers: Relevance to Adhesion," (M. Strobel, C. Lyons, and Mittal, Eds.), p. 3, VSP, Utrecht, 1994.
23. Strobel, M., Walzak, M. J., Hill, J. M., Lin, A., Karbashewski, E., and Lyons, C. S., *in* "Polymer Surface Modification: Relevance to Adhesion," (K. L. Mittal, Ed.), p. 233, VSP, Utrecht, 1996.
24. Thanawala, S. K., and Chaudhury, M. K., *Langmuir* **16,** 1256 (2000), and references therein.
25. Chaudhury, M. K., *J. Adhes. Sci. Technol.* **7,** 669 (1993); Chaudhury, M. K., *Biosens. Bioelectron*. **10,** 785 (1995).
26. Ferguson, G. S., Chaudhury, M. K., Biebuyck, H., and Whitesides, G. M., *Macromolecules* **26,** 5870 (1993).
27. Owen, M. J., and Smith, P. J., *J. Adhes. Sci. Technol.* **8,** 1063 (1994).
28. Hillborg, H., Anker, J. F., Gedde, U. W., Smith, G. D., Yasuda, H. K., and Wilström, K., *Polymer* **41,** 6851 (2000).
29. Vasilets, V. N., Nakamura, K., Uyama, Y., Ogata, S., and Ikada, Y., *Polymer* **39,** 2875 (1998).
30. Ishii, M., and Komatsubara, M., *in* "Proceedings, 1998 IEEE Conf. on Electrical Insulation and Dielectric Phenomena, Atlanta," p. 134, 1998.
31. Huck, T. S. W., Bowden, N., Onck, P., Pardoen, T., Hutchinson, J. W., and Whitesides, G. M., *Langmuir* **16,** 3497 (2000).
32. Koberstein, J. T., and Mirley, C. L., U.S. Patent 5,661,092 (1997); Koberstein, J. T., and Mirley, C. L., U.S. Patent 5,962,079 (1999).
33. Ouyang, M., Yuan, C., Muisener, R. J., Boulares, A., and Koberstein, J. T., *Chem. Mater.* **12,** 1591 (2000).
34. Efimenko, K., and Genzer, J., work in progress.
35. Certain commercial equipment is identified in this article in order to specify adequately the experimental procedure. In no case does such identification imply recommendation or endorsement by the National Institute of Standards and Technology, nor does it imply that the items identified are necessarily the best available for the purpose.
36. Ulman, A., "An Introduction to Ultrathin Organic Films: From Langmuir Blodgett to Self Assembly." Academic Press, New York, 1991.
37. For detailed information about the NIST/Dow Soft X-ray Materials Characterization Facility at NSLS BNL, see: http://nslsweb.nsls.bnl.gov/nsls/pubs/newsletters/Nov96/Dow.html.
38. Fischer, D. A., Mitchell, G. E., Yeh, A. T., and Gland, J. L., *Appl. Surf. Sci.* **133,** 58 (1998); Genzer, J., Sivaniah, E., Kramer, E. J., Wang, J., Koerner, H., Char, K., Ober, C. K., DeKoven, B. M., Bubeck, R. A., Fischer, D. A., and Sambasivan, S., *Langmuir* **16,** 1993 (2000).
39. Stöhr, J., "NEXAFS Spectroscopy." Springer-Verlag, Berlin, 1992.
40. Due to the nature of the polarization dependencies of the NEXAFS signal intensities one cannot distinguish between a completely disoriented sample and a sample whose chains are all tilted by $\approx 55^\circ$, the so called, "magic angle."
41. By carrying the NEXAFS experiments a $\theta = 55^\circ$ we wanted to eliminate any possible influence of the orientation of the various functional groups at the Sylgard-184 surface on the PEY and FY NEXAFS intensities. Several data sets collected at various angles θ indeed confirmed that these surface functionalities were not oriented.
42. Kim, J., Chaudhury, M. K., and Owen, M. J., *IEEE Trans. Dielectr. Electr. Insulation* **6,** 695 (1999).
43. Experiments using scanning force microscopy (Nanoscope III in the tapping mode)[35] revealed that the root-mean square roughness on Sylgard-184

ranged from 0.15 nm (as-prepared) to 0.3 nm (UVO90 treated for 30 mins).
44. Anderson, D. R., *in* "The Analysis of Silicones" (A. L. Smith, Ed.), p. 247. Wiley, New York, 1974.
45. Delman, A. D., Landy, M., and Simms, B. B., *J. Polym. Sci. A* **7,** 3375 (1969).
46. A database of atomic and molecular core edge excitation oscillator strengths, as described by Hitchcock, A. P., and Mancini, D. C., *J. Electron Spectr. Rel. Phenom.* **67** (1994). The oscillator strengths can be downloaded as ASCII data from http://xray.uu.se.
47. Urquhart, S. G., Turci, C. C., Tyliszak, T., Brook, M. A., and Hitchcock, A. P., *Organometallics* **16,** 2080 (1997).
48. Eaborn, C., "Organosilicon Compounds." Butterworths, London, 1960.
49. Chaudhury, M. K., Efimenko, E., and Genzer, J., unpublished data.
50. Foster, M. D., *Crit. Rev. Anal. Chem.* **24,** 179 (1993).
51. Lu, X., Manners, I., and Winnik, M. A., *Macromolecules* **34,** 1917 (2001).
52. Pérez-Bueno, J. J., Ramírez-Bon, R., Vorobiev, Y. V., Espinoza-Beltrán, F., and Gonzáles-Hernández, J., *Thin Solid Films* **379,** 57 (2000).
53. Hillborg, H., and Gedde, U. W., *Polymer* **39,** 1991 (1998).
54. As reported by Kim and coworkers (Ref. 42), these fillers are rarely detected within the first ≈5 nm below the film substrate despite their large concentration in Sylgard-184. In their study, the researchers stated that the above observation did not imply a macroscopic depletion of the filler in the surface region of PDMS. The filler particles could easily be coated by a polymer film of ≈5 nm in thickness and even uncoated and close-packed in the surface they would still constitute only less than 1% of the volume of the top ≈5-nm-thick layer for a flat geometry of special micrometer-sized particles with PDMS filling the interstices.